

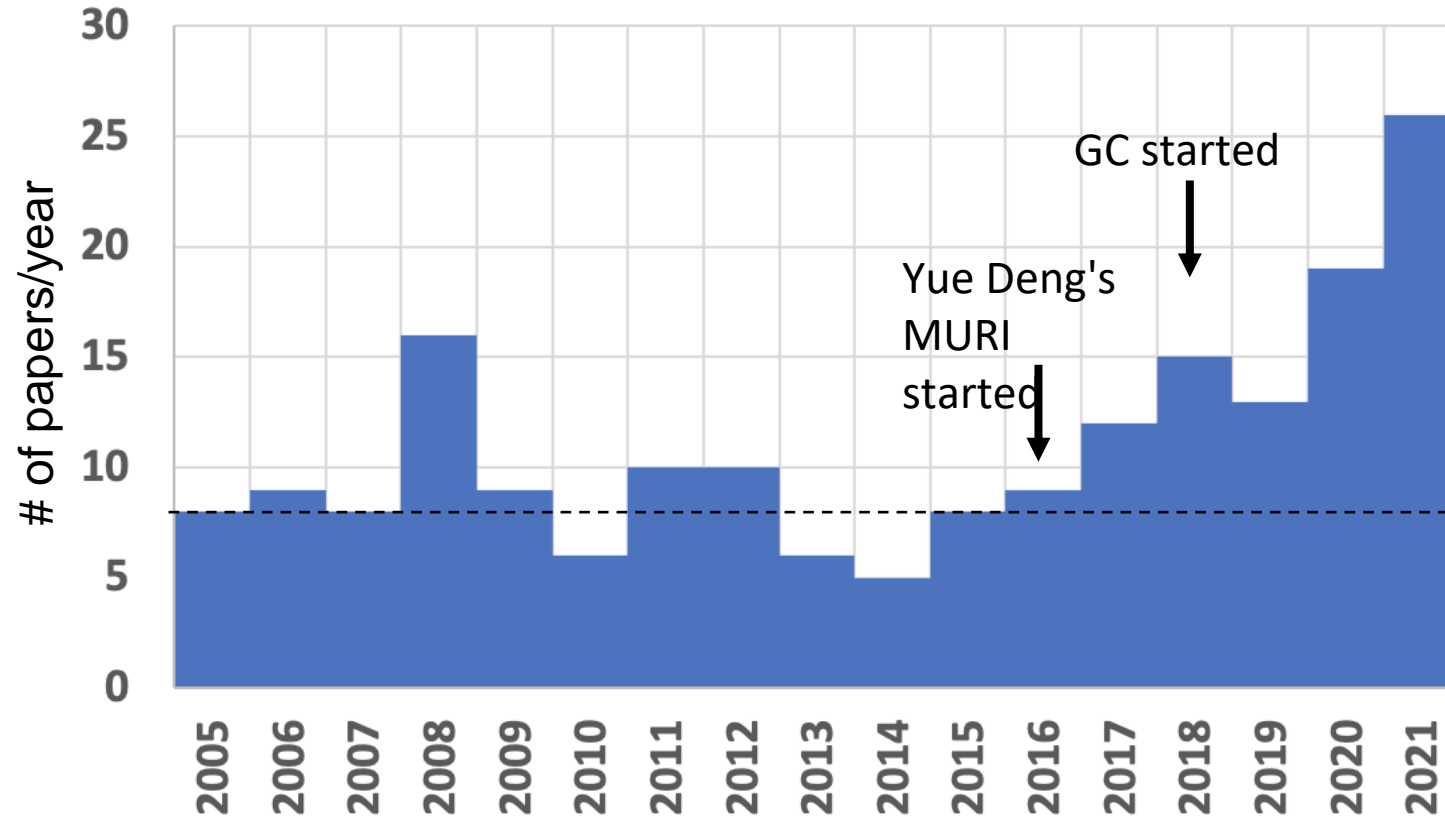
Multiscale IT Dynamics Grand Challenge: Final Report

Aaron Ridley

Toshi Nishimura

(Toshi really pushed this through the years, but couldn't be here)

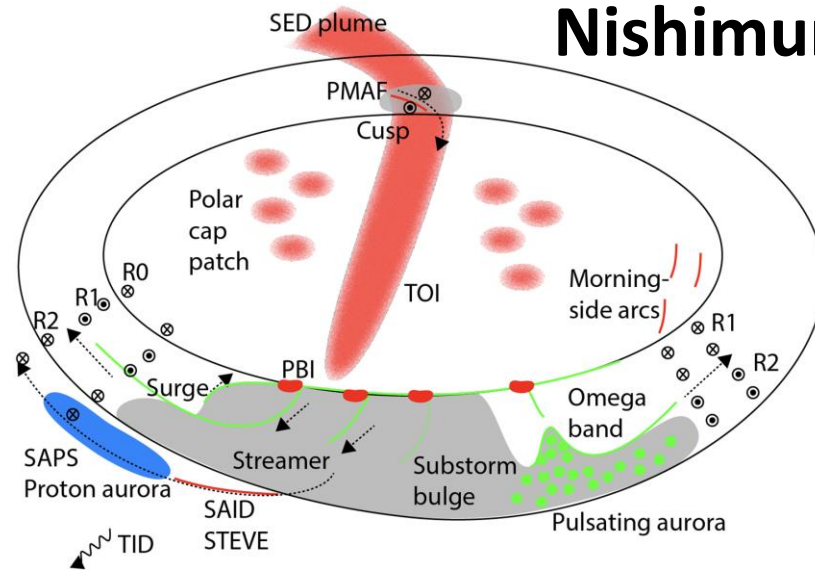
Papers on the multi-scale ionosphere



- Multi-scale ionosphere-thermosphere processes were not popular 5 years ago.
- Now many people talk about multi-scale processes.

Review paper on the importance of multi-scale processes -

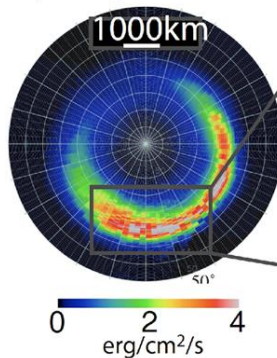
Nishimura



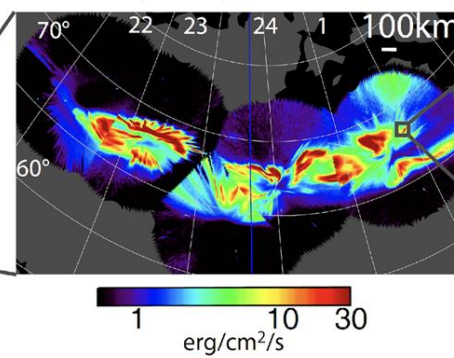
Various types of meso-scale plasma structures exist in the mid and high-latitude ionosphere.

They have multi-scale structures. Meso-scale structures have significant contributions. Small-scale structures are difficult to measure, but they are important for irregularities and dissipation.

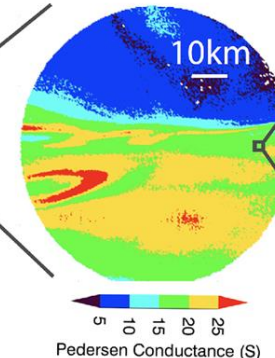
(a) Large-scale (>~1000km) precipitation



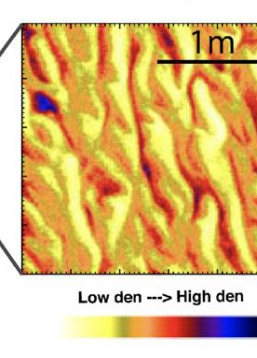
(b) Meso-scale (10s-100s km) precipitation



(c) Small-scale (<~10km) conductance

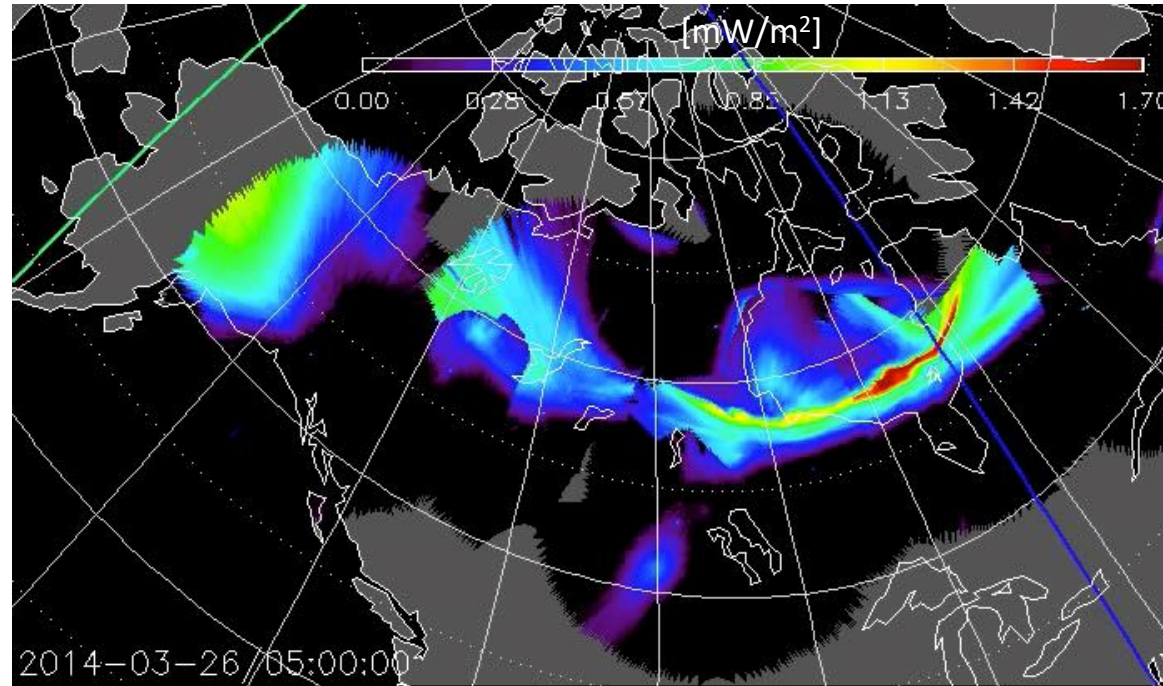


(d) Kinetic scale (<~m) density



Multi-scale precipitation

THEMIS all-sky imagers: Energy flux maps

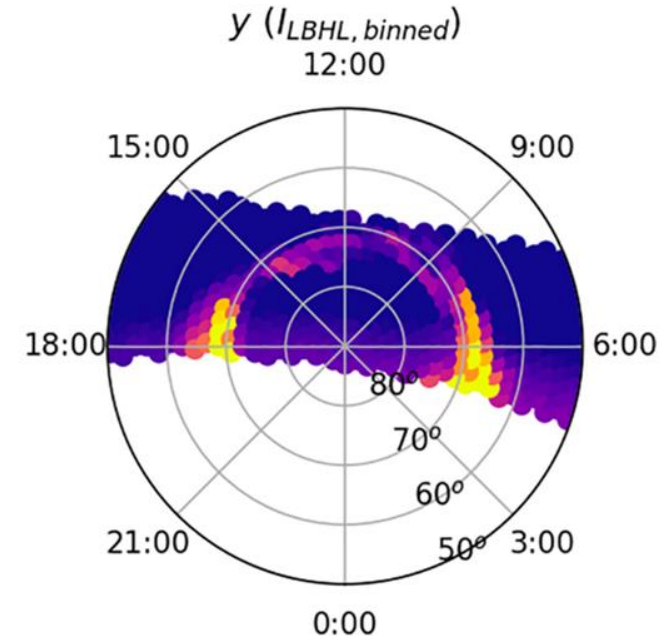
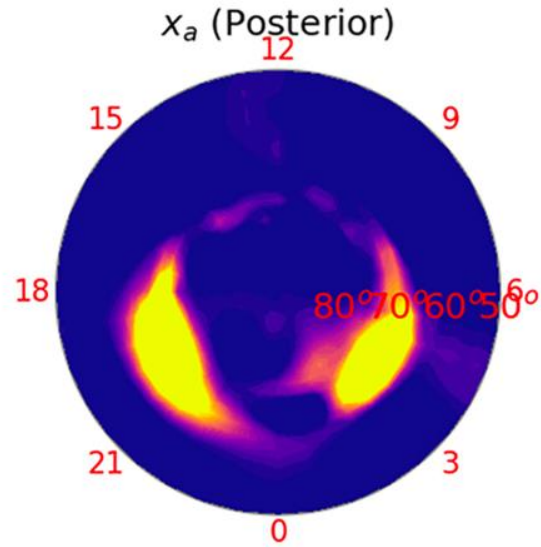
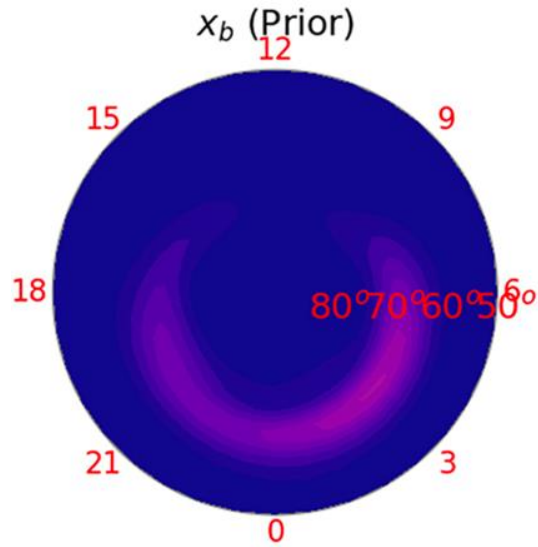


[Nishimura et al., 2021]

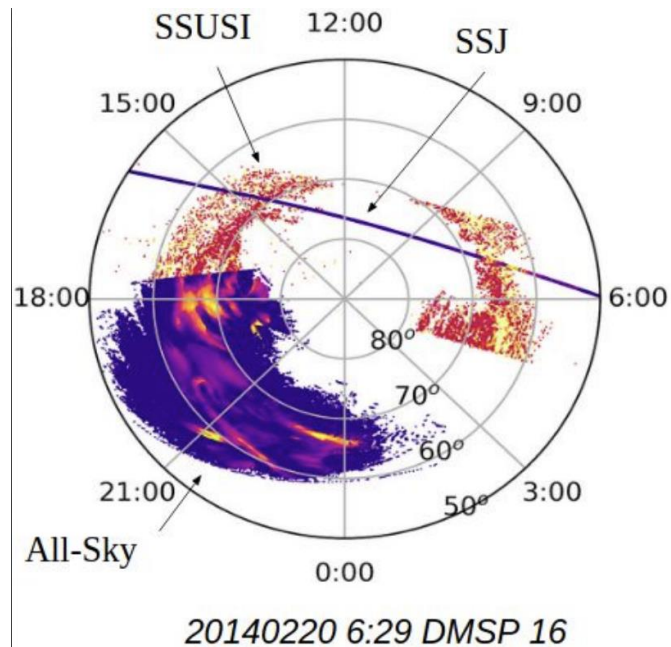
The THEMIS all-sky imager network was used to construct high-resolution maps of precipitating electron energy flux and average energy.

Dynamic evolution of auroral arcs during the substorm has been resolved.

Data assimilation of precipitation

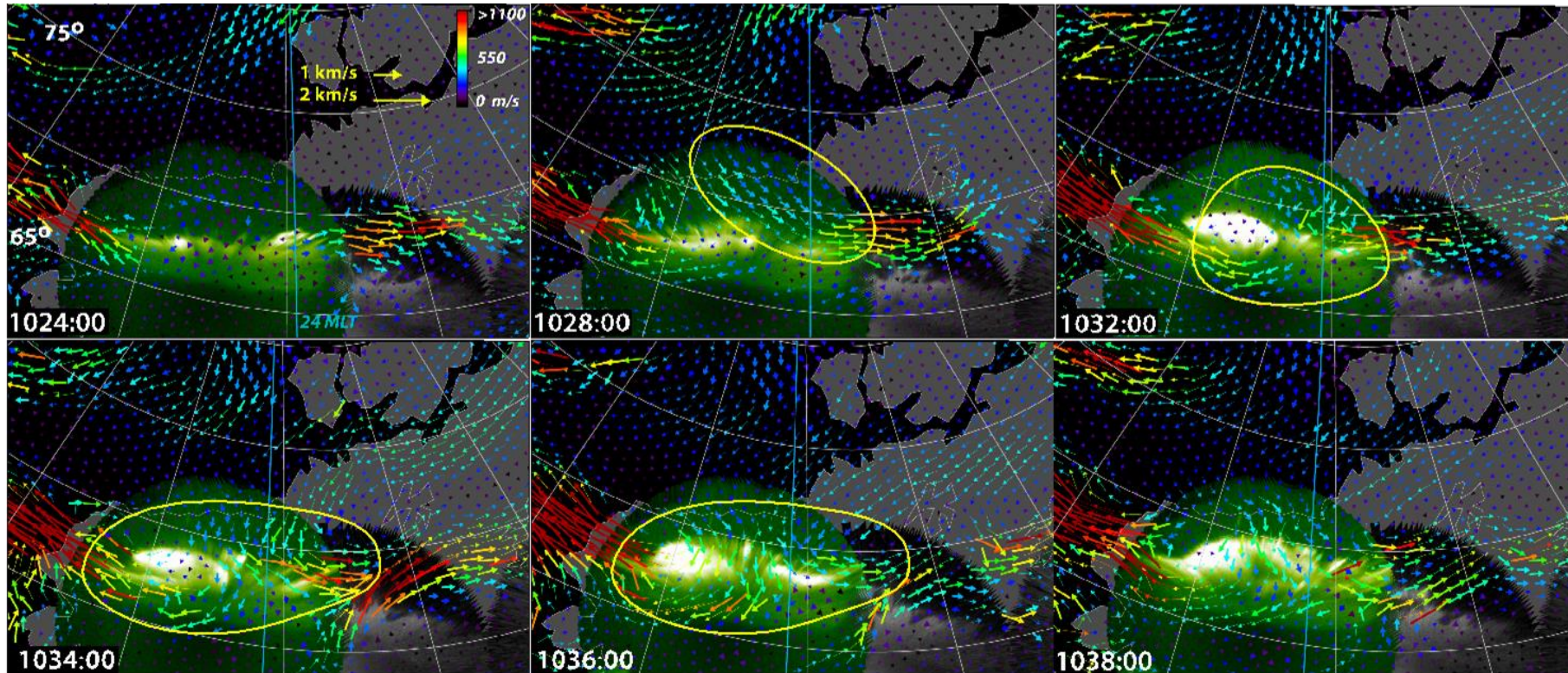


[Li, Matsuo et al., 2022]



A data assimilation model to create a realistic precipitation map with DMSP SSUSI has been developed. The model also plans to incorporate precipitation from the THEMIS all-sky imagers.

Multi-scale convection and aurora - Lyons et al. ; Bristow et al.



[Lyons et al.; Bristow et al.]

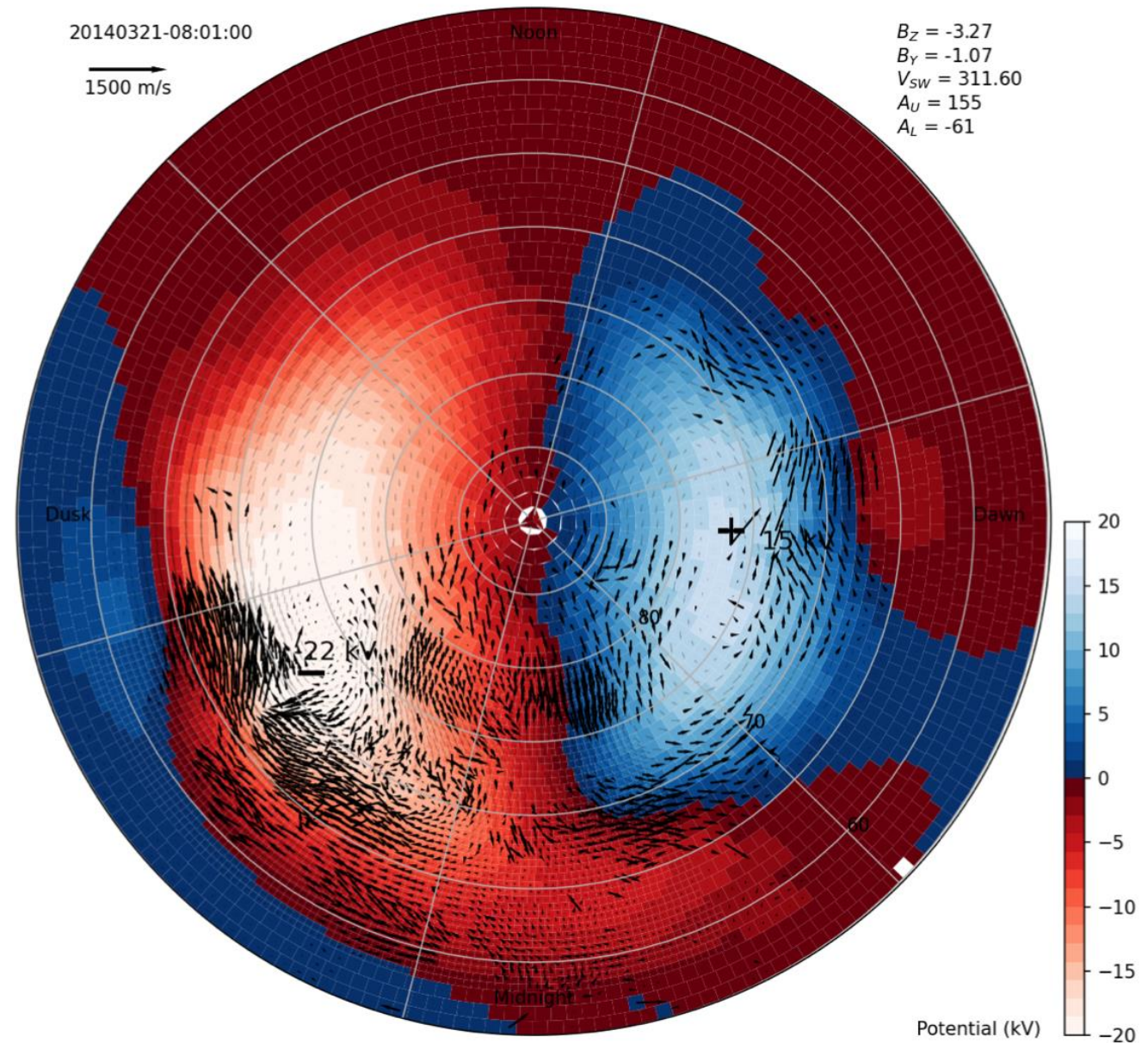
High-resolution flows from SuperDARN reveal meso-scale convection structures that are associated with auroral intensifications during substorms.

Multi-Scale Convection Pattern Estimation - Bristol et al.

al.

Over the period of the Grand Challenge there has been continued development of our capability for estimation of the high-latitude convection pattern. The latest development:

- Calculates the velocity at every point in the domain in a Bayesian inversion that uses:
 - SuperDARN line of sight velocity measurements
 - Assumption that the velocity field is divergence free
 - A machine learning based climatology that varies with A_u , A_l , and SYM-H in addition to the solar wind and IMF.
- Has the ability to incorporate a nested high-resolution region.
- Calculates the potential by integrating the electric field

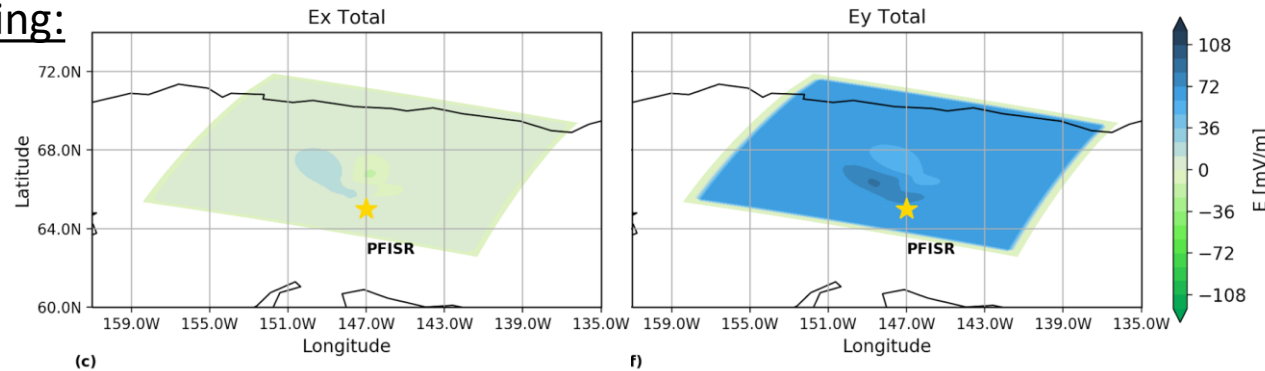


HIME v.01: The treatment of electric fields to resolve meso-scale structures

Dogacan S. Ozturk, Xing Meng, Olga P. Verkhoglyadova, Roger H. Varney, Ashton S. Reimer, Joshua L. Semeter

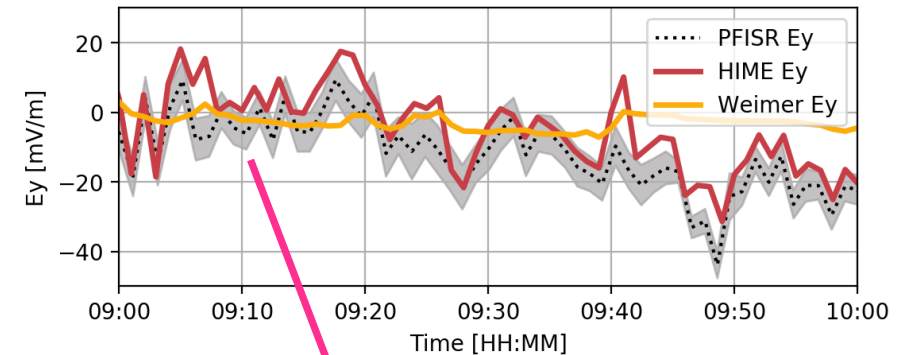
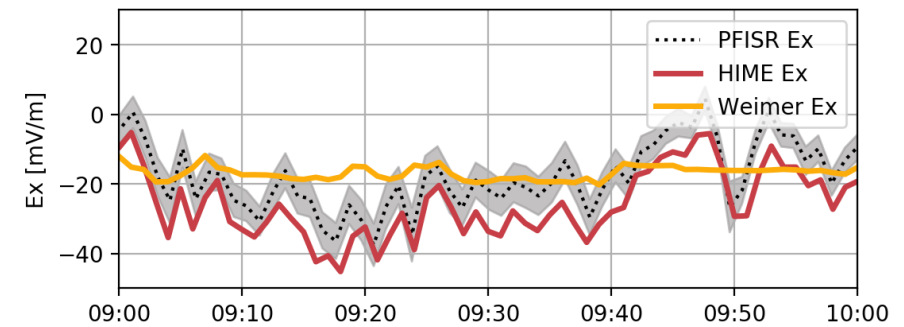
Using down-sampled PFISR 2D electric field estimates, potential differences can be merged with a global empirical potential model to drive global I-T models and investigate the role of meso-scale electric fields.

Down-sampling:



Efield Comparison at 2019-10-26

Latitude = 68.7deg., Longitude = -92.5deg., Altitude = 416.1 km

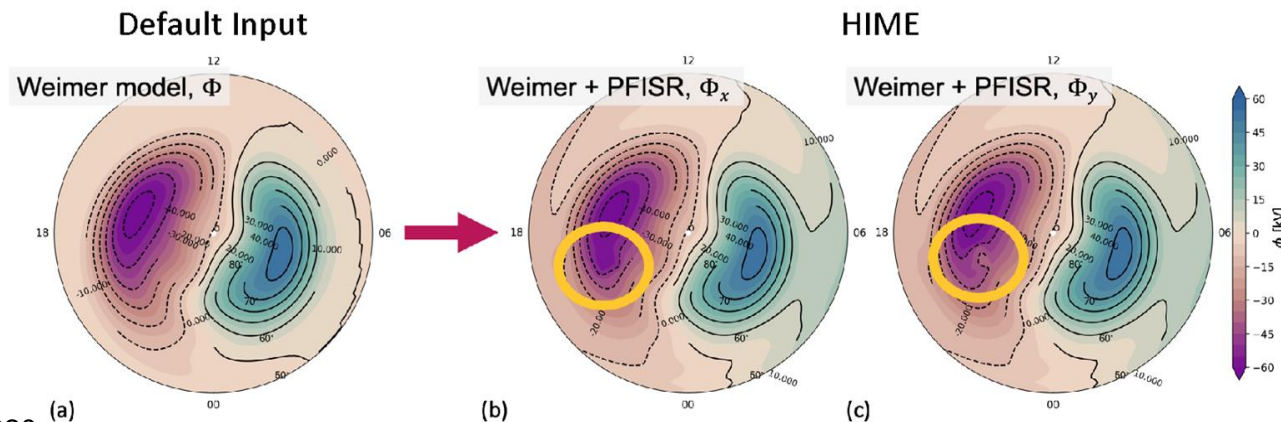


Variability captured in simulations.

Conversion:

$$\Delta\phi_x = - \int_{x_1}^{x_2} E_x dx \quad \Delta\phi_y = - \int_{y_1}^{y_2} E_y dy$$

Merging:



HIME v.02: The treatment of particle precipitation to resolve meso-scale structures

Dogacan S. Ozturk, Xing Meng, Olga P. Verkhoglyadova, Roger H. Varney, Ashton S. Reimer, Joshua L. Semeter

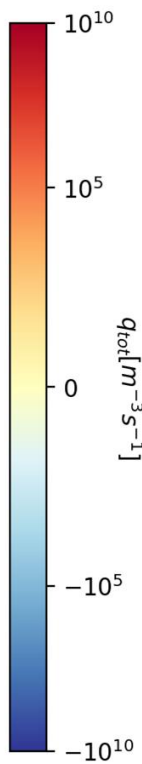
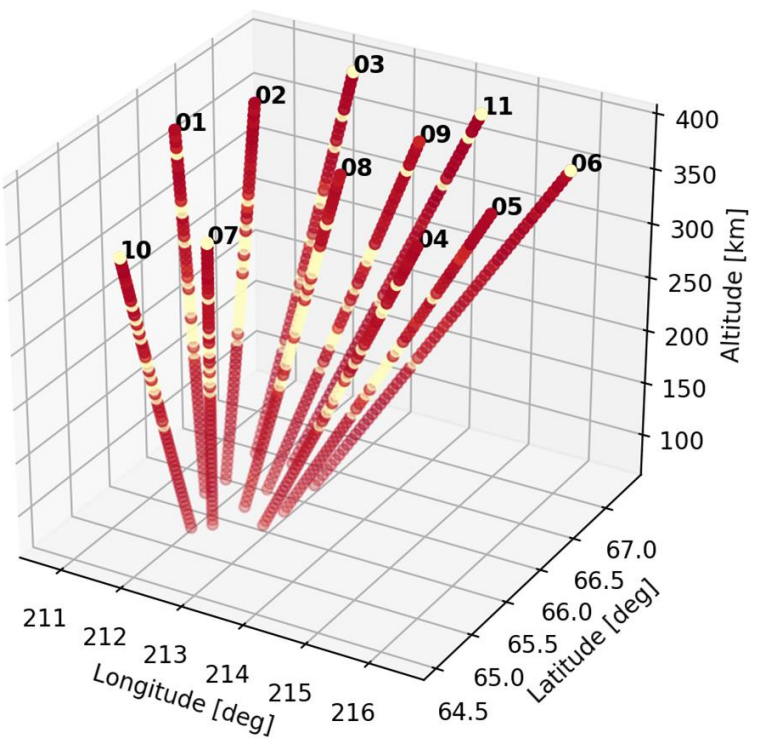
Data-model comparisons help quantify the bulk auroral ionization rates¹.

$$\frac{dn_e}{dt} = \sum_s (q_s - \alpha_s n_s n_e)$$

$$\min. |n_{e,GITM} - n_{e,PFISR}|$$

Corrected bulk auroral ionization rates (q_s) can account for meso-scale precipitation in GCMs.

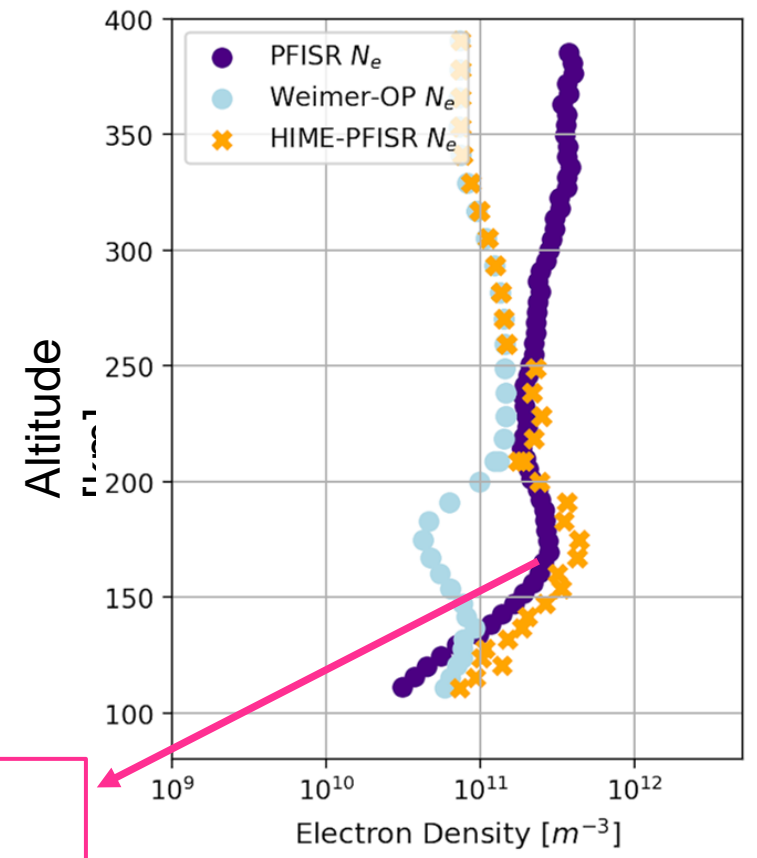
Corrected Auroral Ionization Rate at 06:03UT



Minimizing the difference between simulated and measured electron densities is an optimization problem.

Enhancement captured in simulations.

Beam – 06 at 06.03 UT

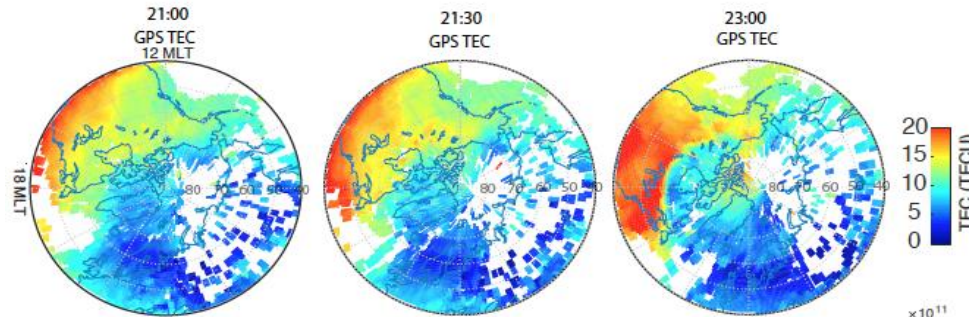


1 [Rees, M.H., 1989]

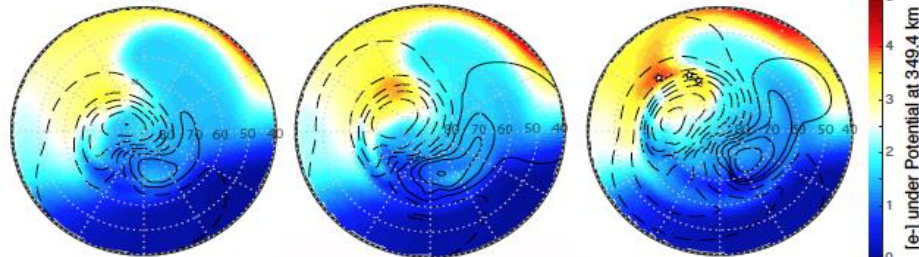
* Purple dots show averaged electron density values. A cut-off applied at 250

Polar Cap Patch: **Formation**, Evolution and Impact - Wang & Zou et al.

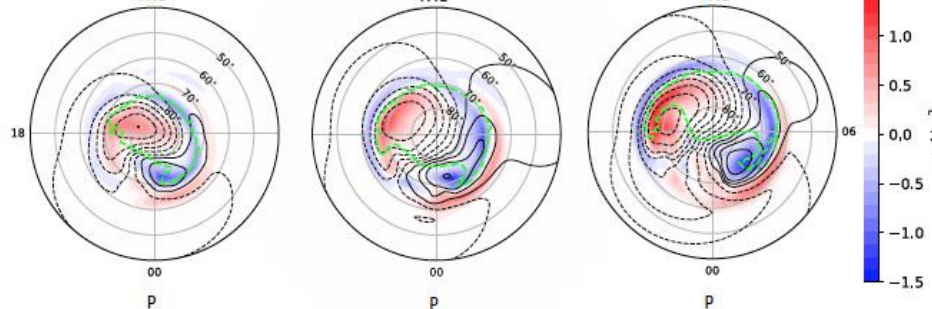
GPS TEC



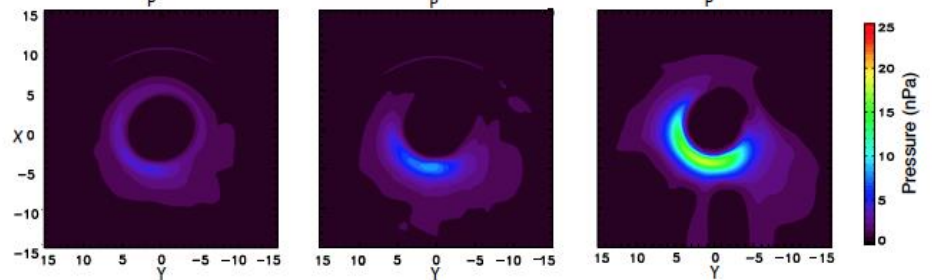
GITM Ne at 350 km



IE electrodynamics



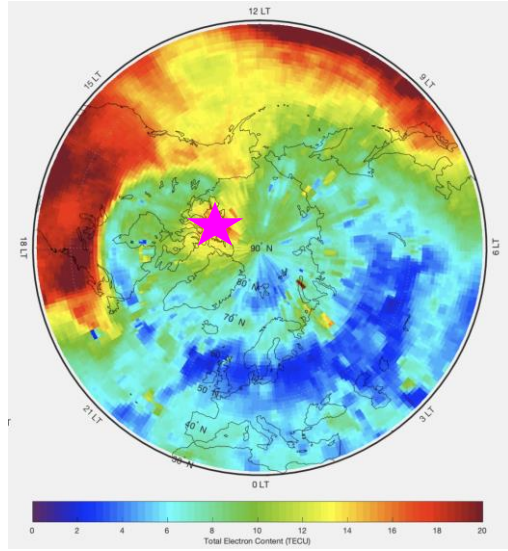
BATSRUS plasma pressure



- Plasma was lifted to higher altitudes mainly due to projection of the northward convection flows in the vertical direction.
- **Enhanced boundary flows led to the increased frictional heating and electron density decrease, i.e., segmenting the SED plume into a patch.**
- Convection electric fields penetrated to lower latitudes;
- West drifting partial ring current increased shielding and Region-2 FACs;
- Closure of Region 1 and 2 FACs led to large boundary flow.
- Partial ring current formed and drifted westward after the storm initiated.

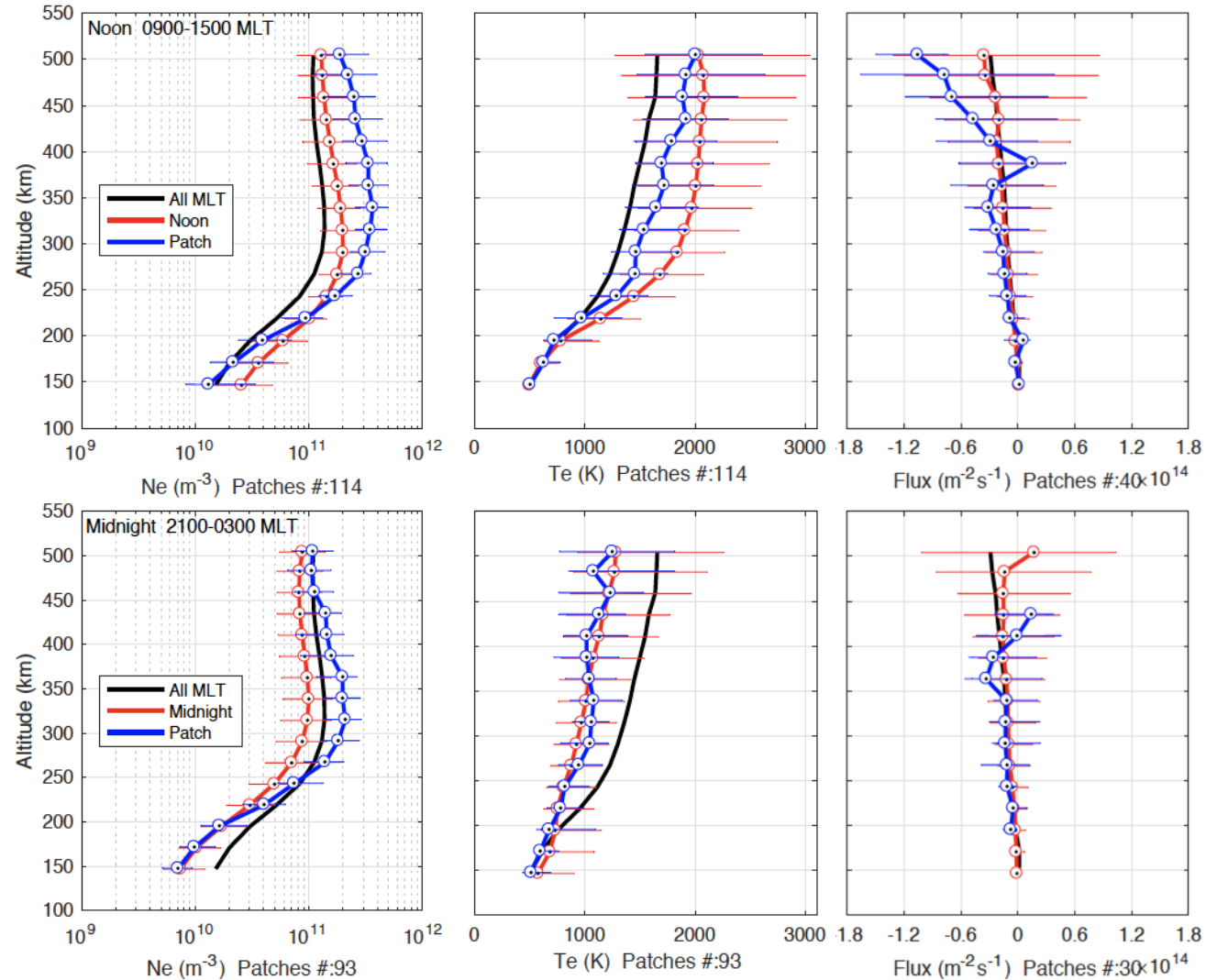


Polar Cap Patch: Formation, Evolution and Impact - Ren & Zou et al.



Superposed Epoch Analysis of Polar Cap Patch

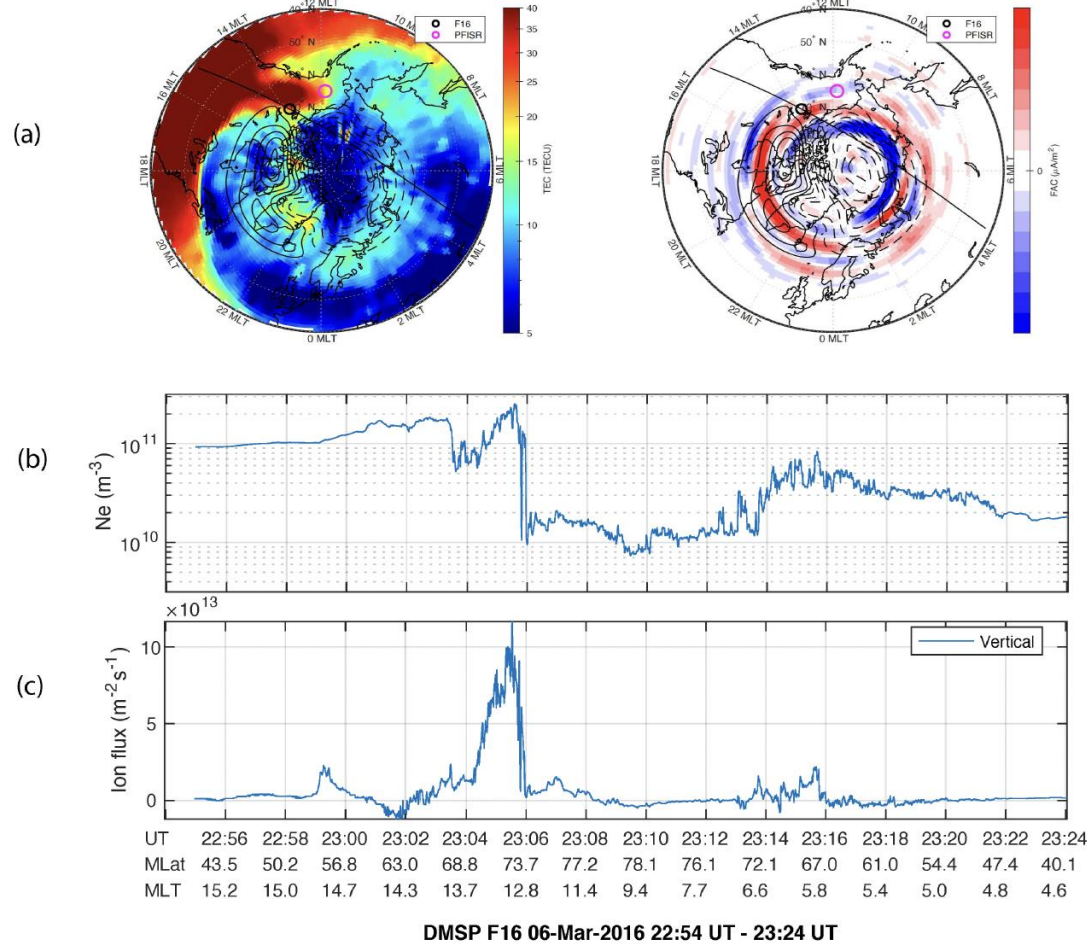
- Denser and cooler plasma than surrounding region
- Demonstrated the solar produced SED plume plasma as main source for patch
- Downward plasma flux in the polar cap



Ren, J., Zou, S., Gillies, R. G., Donovan, E., & Varney, R. H. (2018). JGR

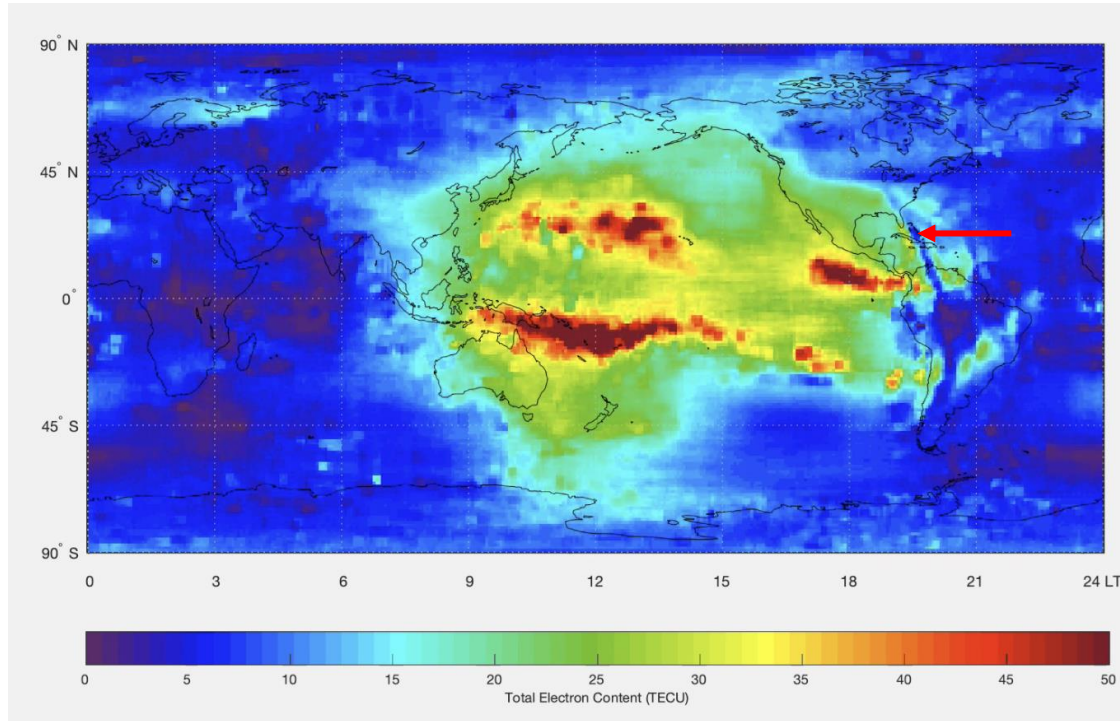
Polar Cap Patch: Formation, Evolution and **Impact** - Zou et al.

06-Mar-2016
23:04:00



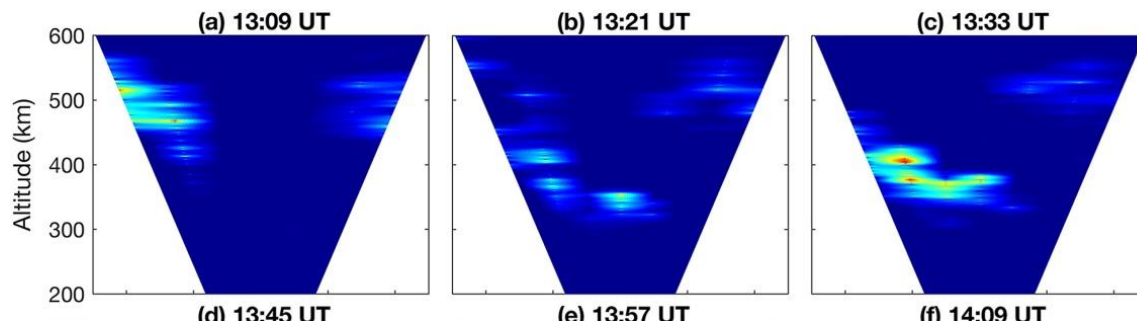
- Evolution of ionospheric density structures strongly affect the ion upflow fluxes.
- Even under similar convection and particle precipitation conditions, the reduced ionospheric density during the negative storm phase led to weakened upward fluxes.
- Dynamic processes in the coupled ionosphere-thermosphere system and the resulting state of the ionospheric storm are crucial for understanding the temporal and spatial variations of ion upflow fluxes and thus should be incorporated into coupled geospace models for improving our holistic understanding of the role of ionospheric plasma in the geospace system.

Super Equatorial Plasma Bubble - Aa et al.



- Equatorial plasma bubbles can extend to higher latitudes than previously expected, e.g., reaching equatorward boundary of mid-latitude trough.
- New space weather challenge for continental US.

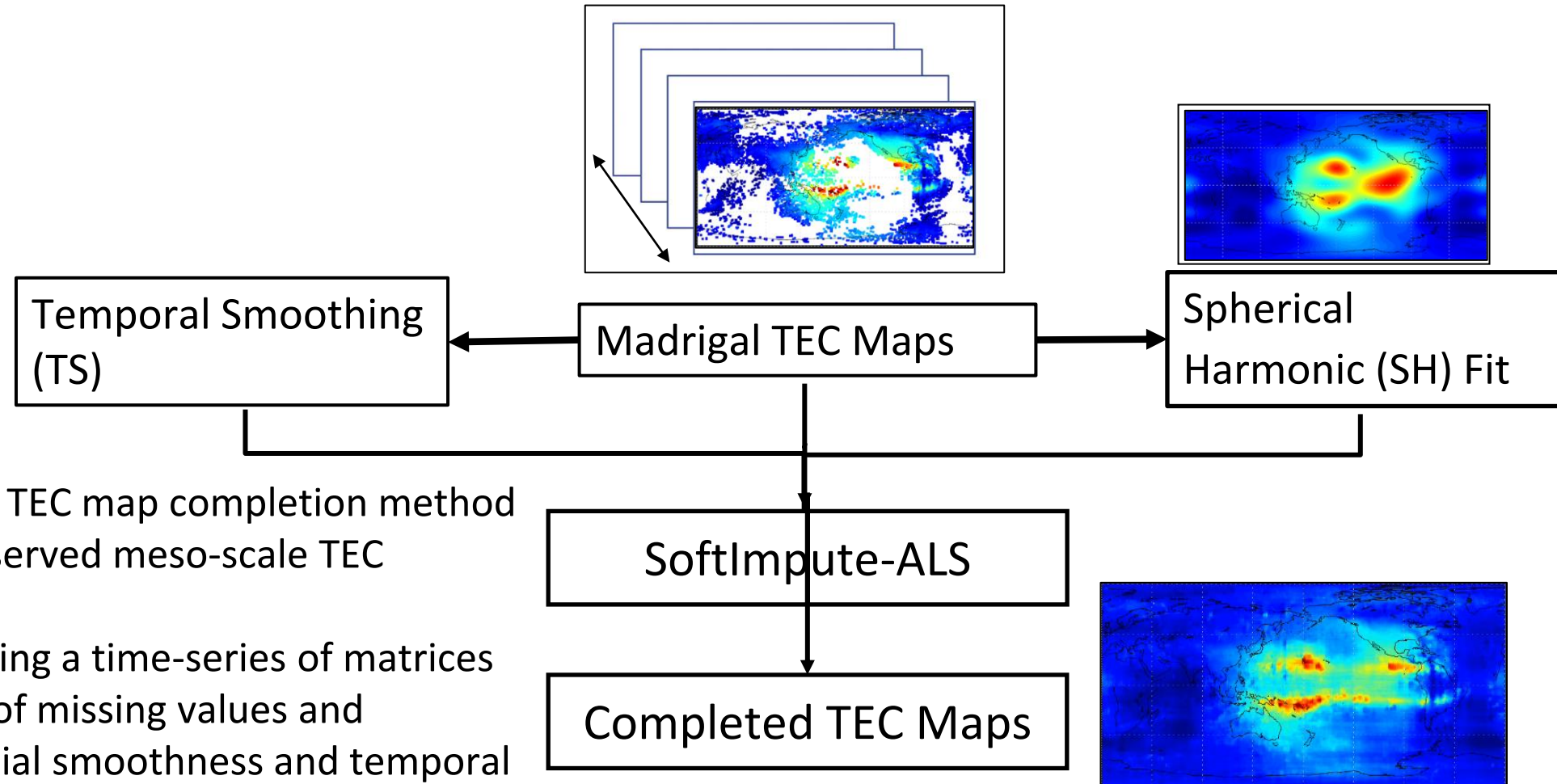
“Baby” EPB revealed by HF phased array radars



Aa, E., Zou, S., Ridley, A. J., Zhang, S.-R., Coster, A. J., Erickson, P. J., et al. (2019). *Space Weather*.

Jin, H., Zou, S., Chen, G., Yan, C., Zhang, S., & Yang, G. (2018). *Space Weather*.

Multi-scale Ionospheric Density Structures Revealed in Global TEC map - Sun et al.

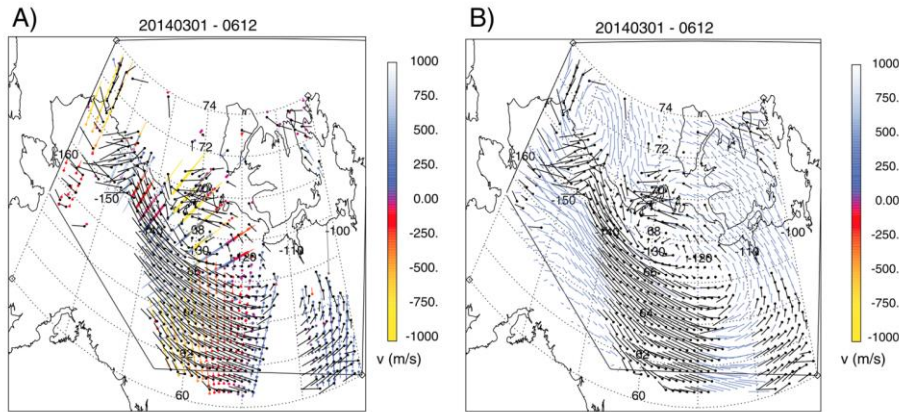


- VISTA is a new global TEC map completion method that can *preserve* observed meso-scale TEC structures.
- It is capable of inputting a time-series of matrices with a large amount of missing values and guarantees both spatial smoothness and temporal consistency, particularly useful for reconstructing scientific images, i.e., the TEC maps/videos.

Sun, H., Hua, Z., Ren, J., Zou, S., Sun, Y., Chen, Y. (2021) Annals of Applied Statistics.

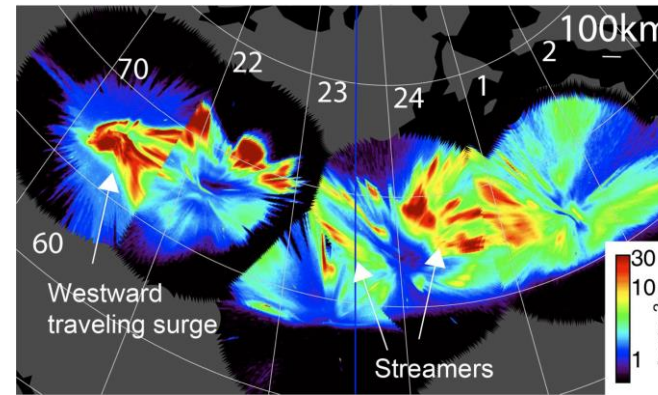
Utilize high-res convection and precip maps to drive GITM for real event study - Sheng et al.

High-res SuperDARN Convection



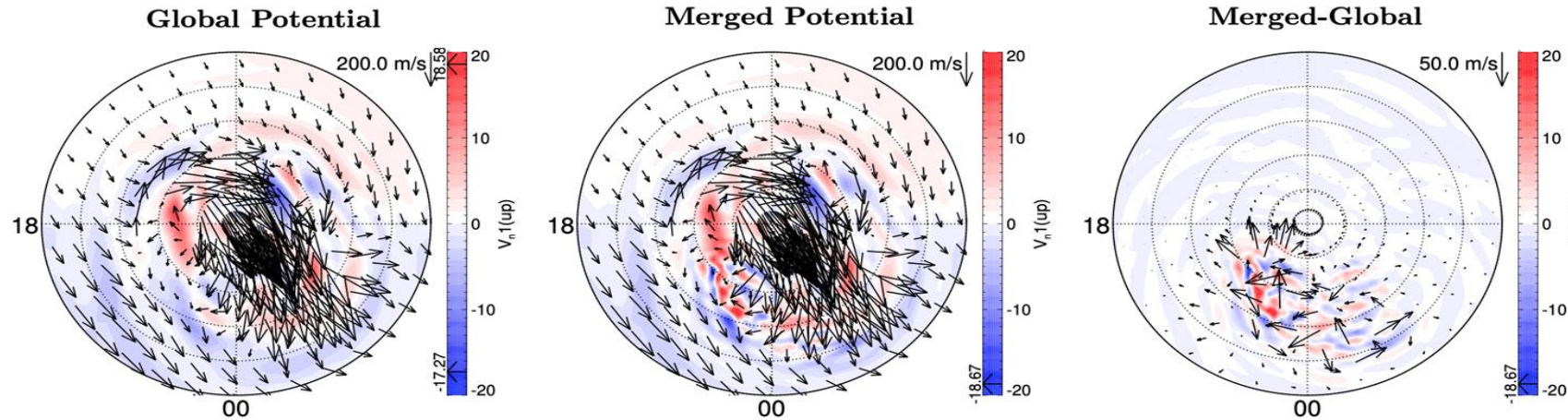
[Bristow et al., 2016]

High-res ASI Precipitation Map



[Courtesy of Toshi]

GITM – Neutral Winds



- Vertical (color) and horizontal winds (vector) at 07:30:00 UT
- High-resolution convection \square Meso-scale structures in neutral dynamics

[Sheng et al., To be submitted]

GITM with local-mesh refinement applied to a Typhoon event simulation - Zhao / Deng et al.

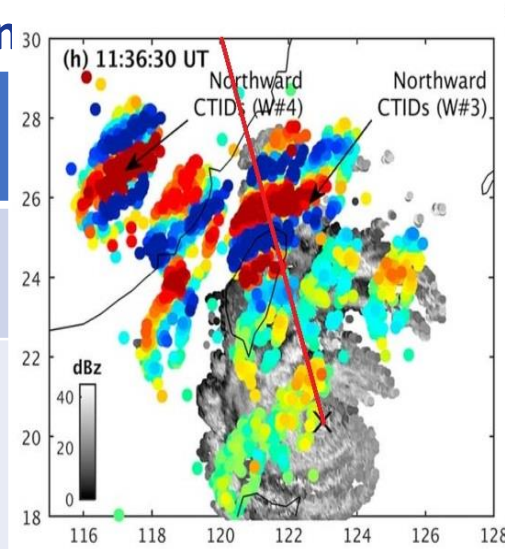
- Achieve high resolution in the regional domain
- Improve boundary conditions to regional domain

Simulation: Typhoon Meranti in 2016

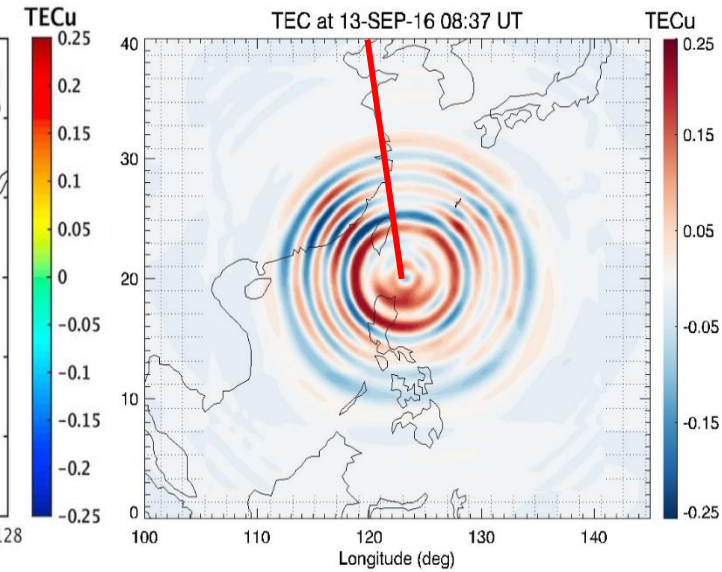
Compare of TEC perturbation

	GNSS dTEC	GITM-R dTEC
Amplitude (TECu)	0.25	0.15
Horizontal Wavelength h (km)	170	200

GPS dTEC



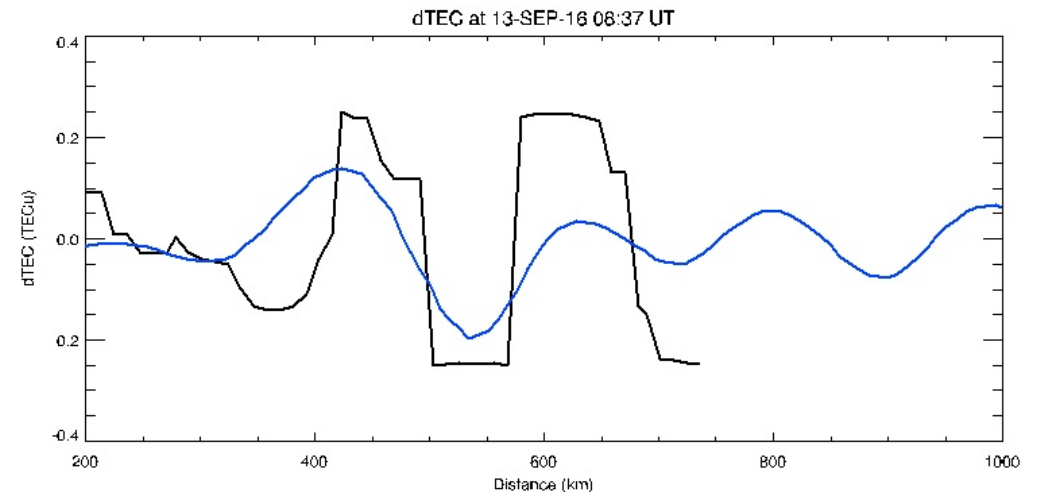
GITM-R dTEC



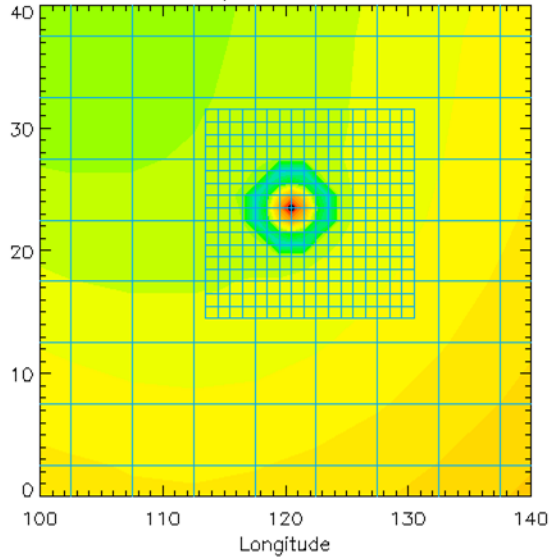
[Chou et al., 2017]

- Simulation is consistent with observation in **wave length** and **amplitude**.

[Zhao et al., 2020]



LGR, Temperature at 100 km



Example:
 regional: $1^\circ \times 1^\circ$
 Global: $5^\circ \times 5^\circ$

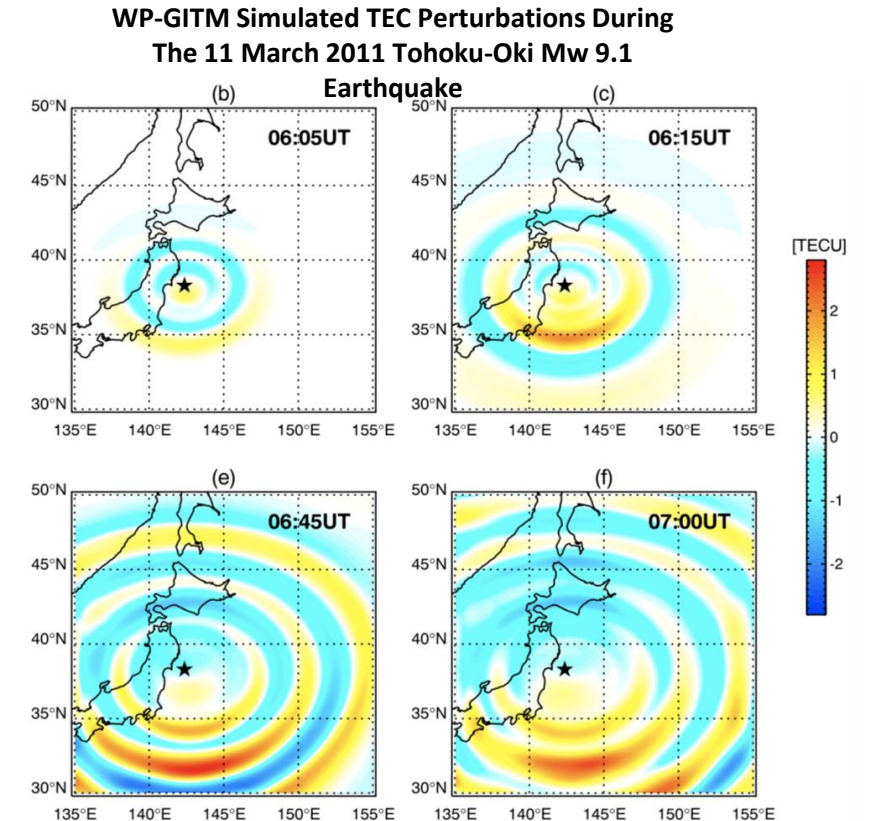
[Deng et al., 2021]

WP-GITM (Earthquake Reaction) Research Highlights - Meng et al.

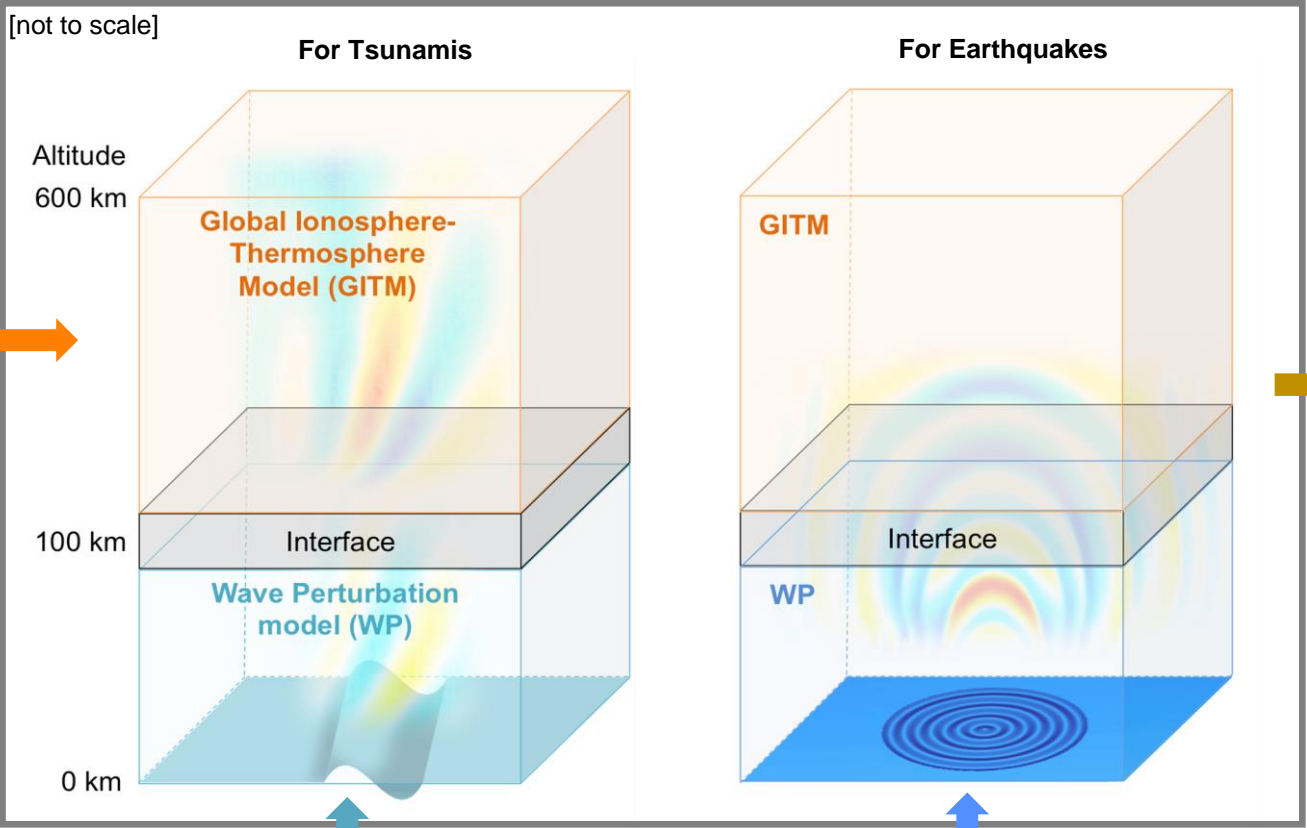
- Over the past 5 years, the tsunami-ionosphere coupling model Wave Perturbation-GITM (WP-GITM) has been extended to address the earthquake-ionosphere coupling, capturing the atmospheric acoustic-gravity waves induced by both the epicentral crustal motion and the propagating seismic waves.
- We validate WP-GITM with GPS TEC data for a number of earthquake events and find good agreements.
- The advancement of WP-GITM enables the quantification of the seismic versus non-seismic contributions to the distribution of the co-seismic ionospheric disturbances.

References:

- Meng, X., Verkhoglyadova, O. P., Komjathy, A., Savastano, G., & Mannucci, A. J. (2018). Physics-based modeling of earthquake-induced ionospheric disturbances. *JGR*, 123, 8021–8038.
- Meng, X., Ravanelli, M., Komjathy, A., & Verkhoglyadova, O. P. (2022). On the north-south asymmetry of co-seismic ionospheric disturbances during the 16 September 2015 Illapel M8.3 earthquake. *GRL*, 49, e2022GL098090.



WP-GITM Infrastructure



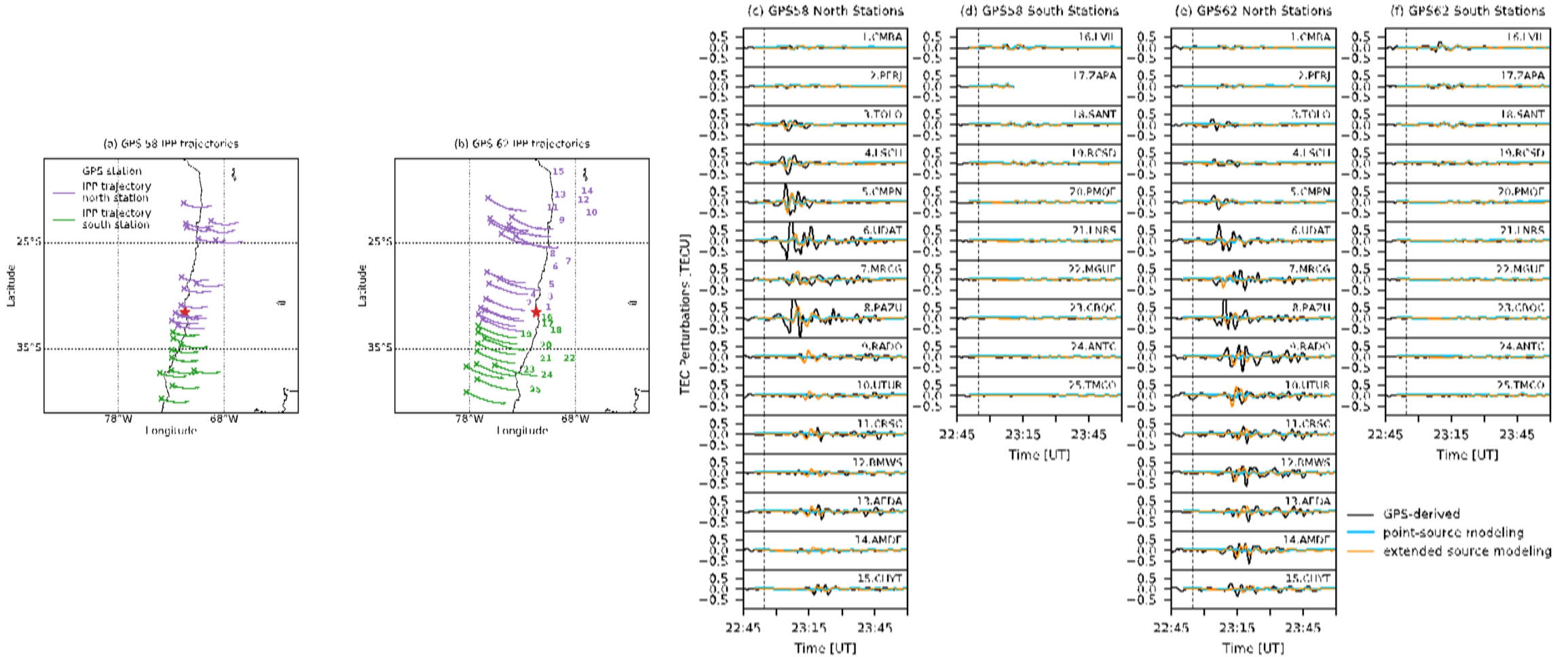
Input I
solar wind conditions, solar irradiance, auroral particle precipitation

Input II
tsunami wave characteristics

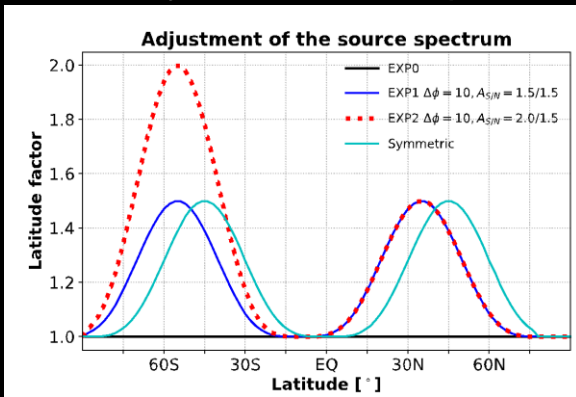
Input II
surface vertical velocity from seismic data

Output
Disturbances in ionospheric and thermospheric variables

WP-GITM-simulated Vs GPS-derived TEC Perturbations for 16 September 2015 Illapel Earthquake

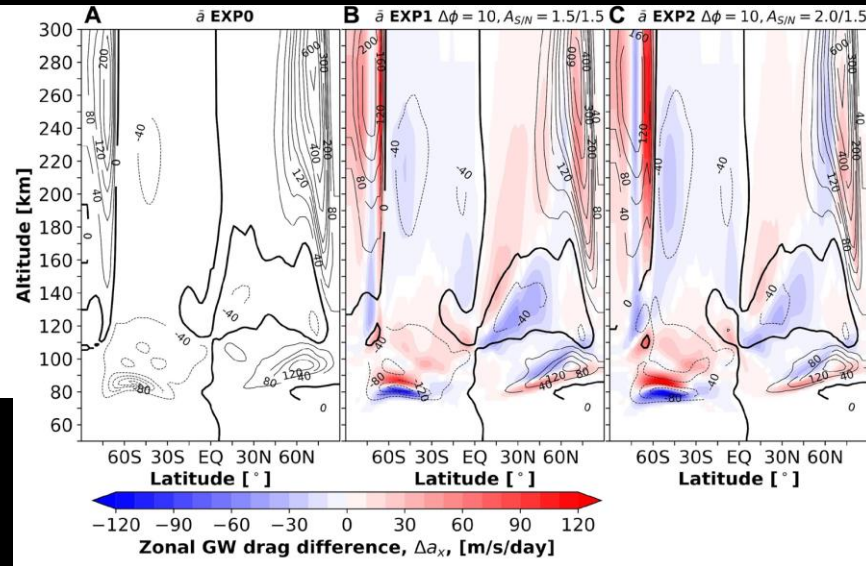


Gravity wave source spectrum

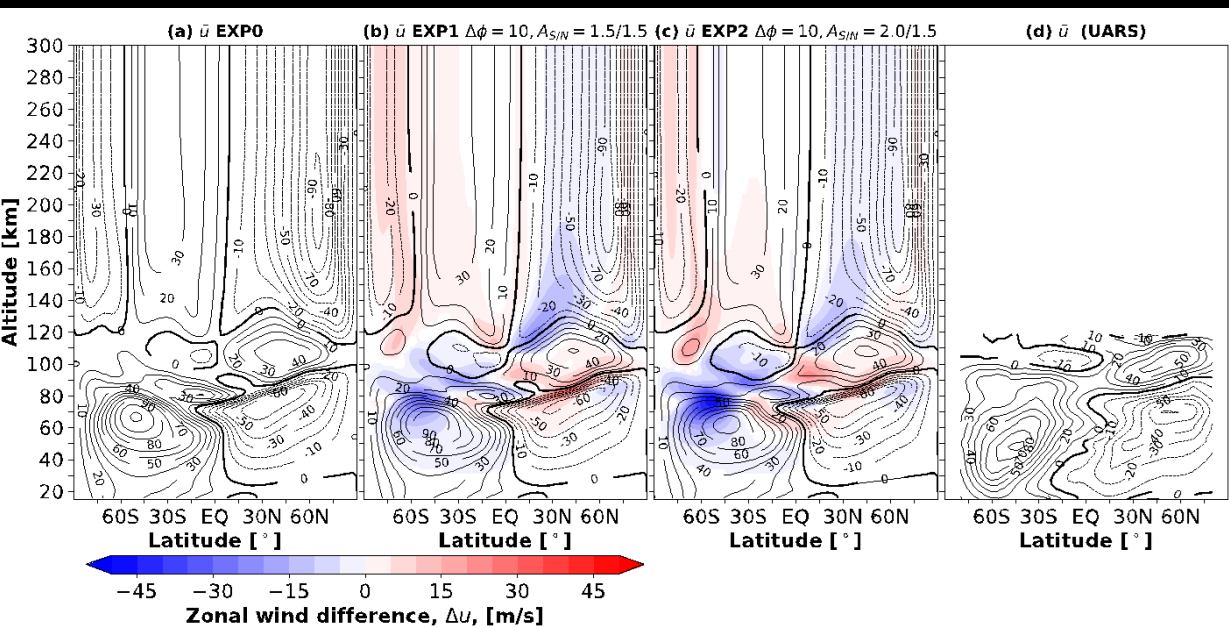


(Yigit et al., 2021, FASS, <https://doi.org/10.3389/fspas.2020.614018>)

Mean gravity wave drag



Mean zonal winds

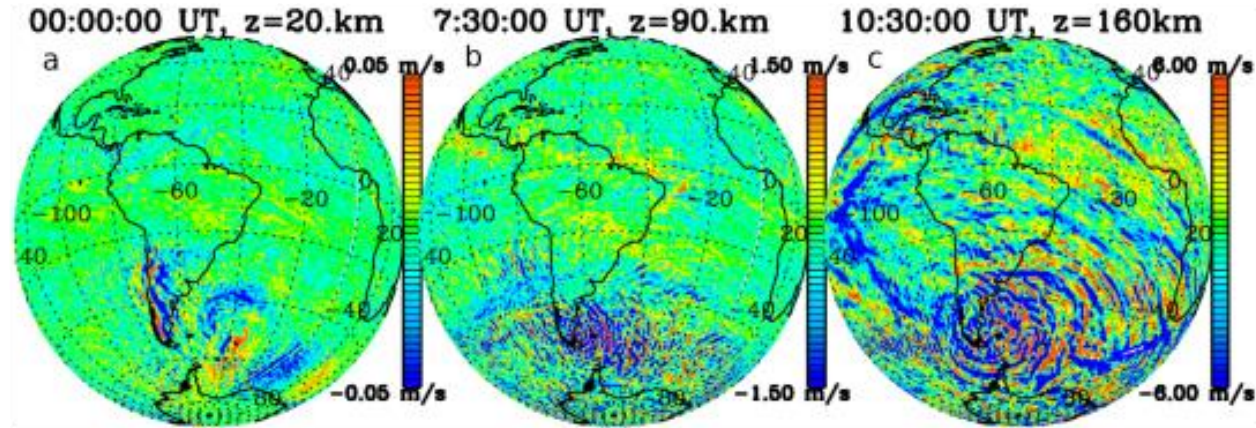


CMAT2 simulations of thermospheric GW effects using the whole atmosphere GW parameterization (Yigit et al., 2008, JGR)

Modeling the effects of latitudinal variations in gravity wave source activity in the upper atmosphere for June/July 2010.

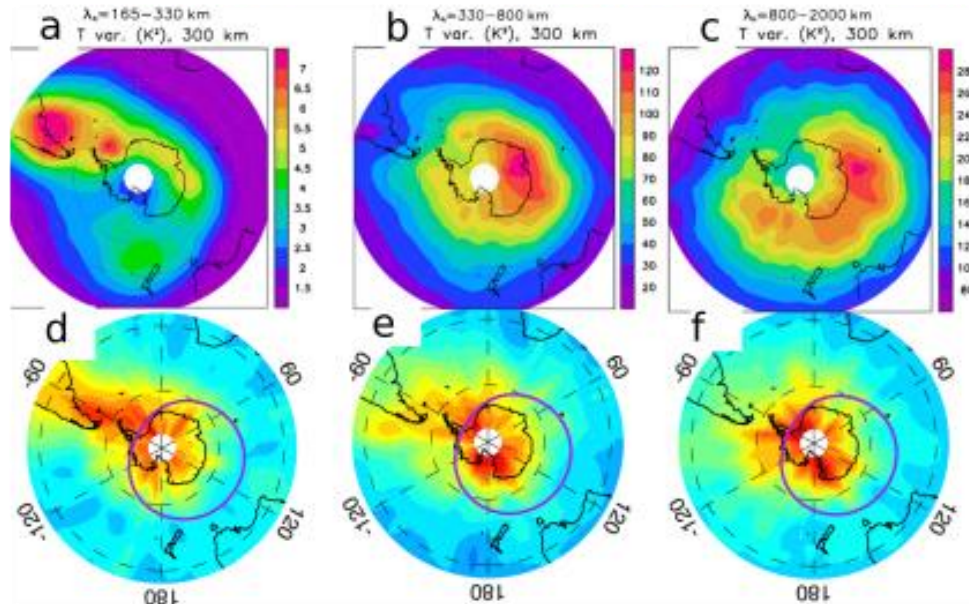
- EXP0: benchmark, uniform global distribution of the maximum gravity wave source strength
- EXP1: Southward shifted (by 10°) sinusoidal spectrum; max source strength increased 50%.
- EXP2: Same as EXP1, Max source strength increased by 100% in Northern Hemisphere and 50% in Southern Hemisphere.
- Difference in mean wind and GW drag calculated by subtracting the benchmark case from EXP1 and EXP2.
 - Thermospheric mean GW drag up to 600 m/s/day, peaking at high latitudes
 - Latitudinally varying spectra produce more realistic wind distributions

During the last 5 years, the bar has risen significantly for simulating realistic GWs in the thermosphere from lower atmospheric sources. We are now not only able to simulate more-realistic GWs from specific events (orographic, polar night jet) using the The High Altitude Mechanistic general Circulation Model (HIAMCM), but we are also able to compare well with observed data for these events. Here, the large scales in the HIAMCM are nudged to the background wind and temperature from MERRA-2



Orographic forcing:

A strong mountain wave (MW) event over the Southern Andes during July resulted in secondary Gws in the MLT and tertiary GWs in the thermosphere/F region using the free-running HIAMCM (Vadas & Becker, 2019)

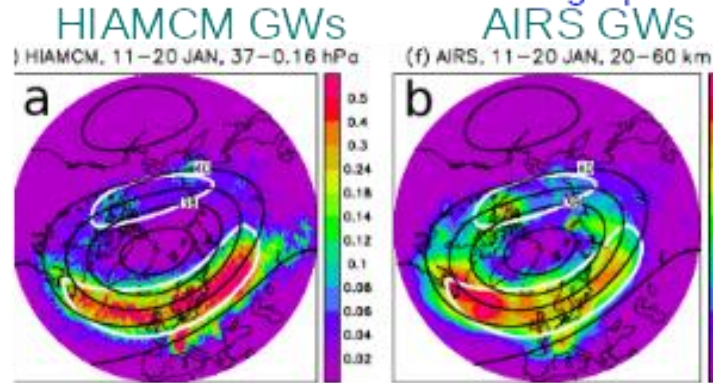


HIAMCM GWs
(Becker & Vadas, 2020)

GOCE Gws
(Xu et al, 2021)

These orographically-forced tertiary GWs agree well with the GW hotspot seen over the Southern Andes in GOCE and CHAMP data

We are now also able to reproduce the AIRS GWs using the nudged HIAMCM! These GWs are from jets and orographic forcing

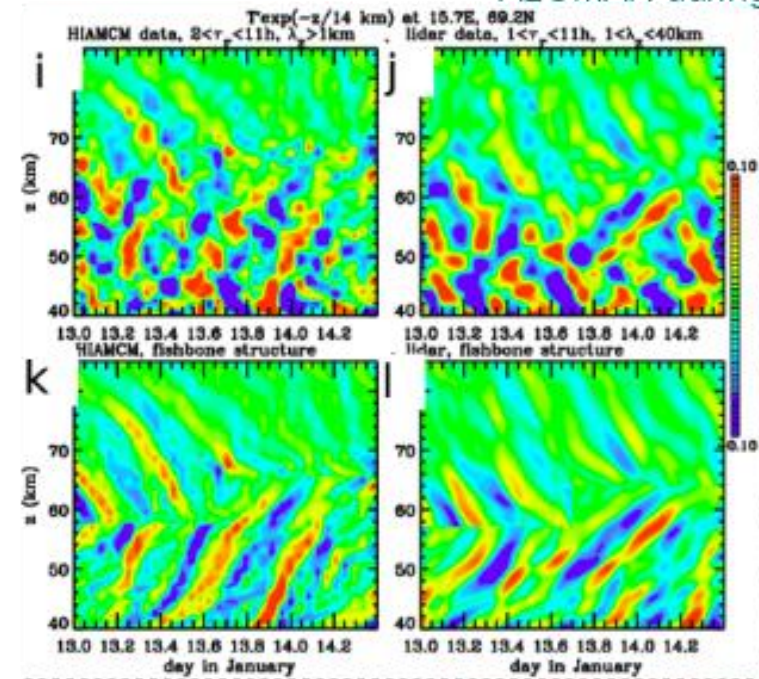


We are also now able to reproduce lidar data at ALOMAR Observatory showing the secondary GWs excited by the breaking and dissipation of primary GWs excited by the stratospheric polar vortex

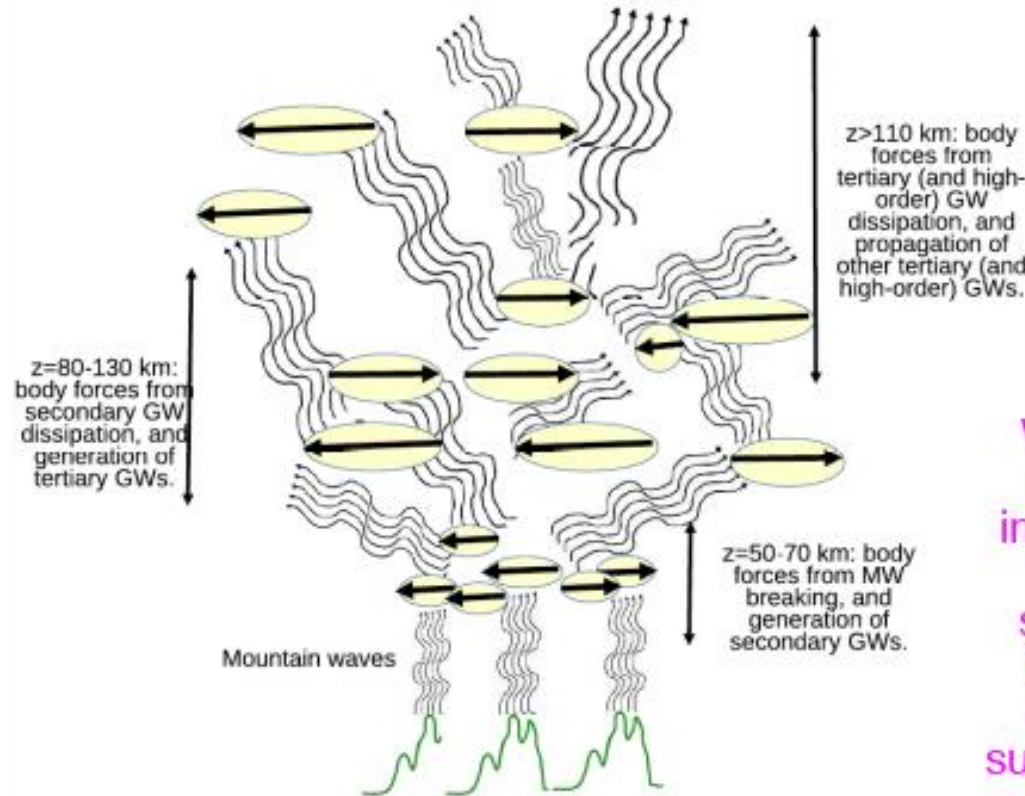
HIAMCM secondary GWs over ALOMAR on 13-14 January 2016

GWs observed by lidar at ALOMAR during same event

(Becker et al, 2022)



(Vadas et al, under review)



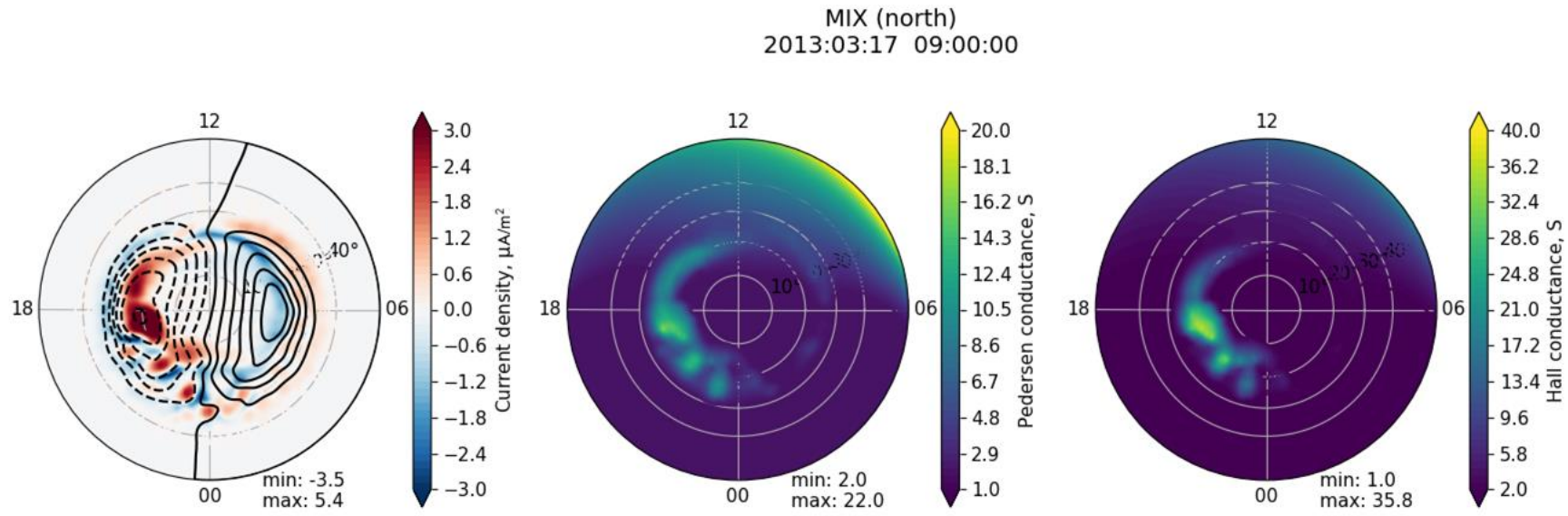
We now know that GWs in the wintertime thermosphere can only be understood by including multi-step vertical coupling, whereby primary GWs dissipate, thereby exciting secondary GWs, etc. This is because these wintertime GWs have very small horizontal phase speeds, and are not fast enough to survive damping from molecular viscosity in the thermosphere.

Turbulence modified by Precipitation - Oppenheim et al.

- What happens to regions with Farley-Buneman (FB) turbulence during precipitation?
 - Without Precipitation, FB waves start when:
 - $\frac{E_{mag}}{B_0} \approx V_D > \approx C_s \left(1 + \frac{v_e v_i}{\Omega_e \Omega_i}\right)$
 - This leads to anomalous conductivity.
 - With Precipitation
 - Temperatures rise so C_s increases.
 - A full kinetic analysis shows that the effect is larger than this.

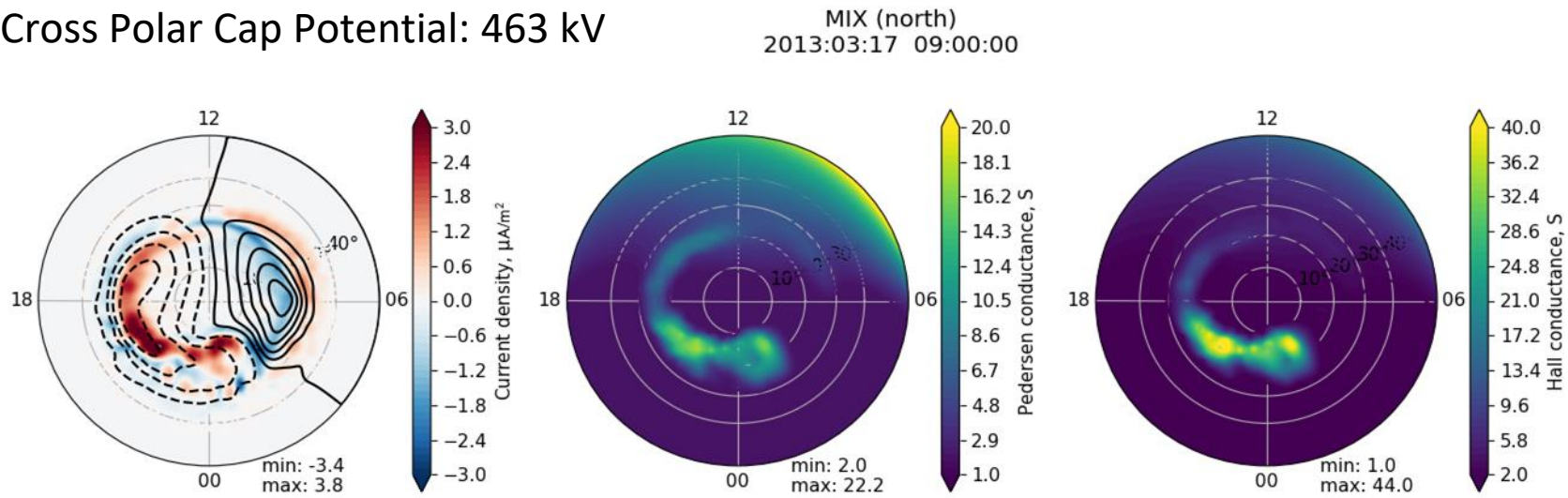
Fully coupled LFM-MIX-RCM-TIEGCM simulation of the 2013 St. Patrick's Day storm - Merkin et al.

Without ET



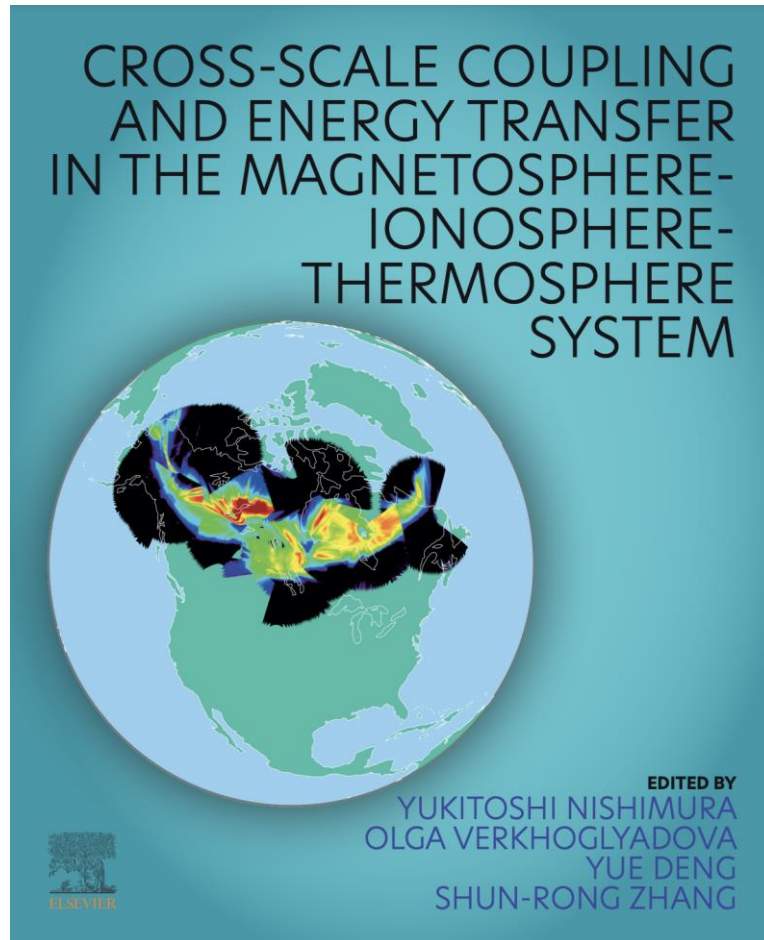
Cross Polar Cap Potential: 463 kV

With ET



Cross Polar Cap Potential: 383 kV

Review Book in Elsevier: Cross-Scale Coupling and Energy Transfer in the Magnetosphere-Ionosphere-Thermosphere System



Editors: Toshi Nishimura, Yue Deng,
Olga Verkhoglyadova, and Shunrong Zhang

Published in December 2021

We thank 49 authors who have contributed to this book.

The book is not a collection of papers but extensively reviews basic concepts and current understanding.

<https://www.elsevier.com/books/cross-scale-coupling-and-energy-transfer-in-the-magnetosphere-ionosphere-thermosphere-system/nishimura/978-0-12-821366-7>

AGU Fall Meeting sessions (2018-)

The screenshot shows a Zoom meeting interface. At the top, there are video thumbnails for Toshi Nishimura, Astrid Maute, and Rafael Mesquita. The main content area displays a presentation slide titled "Combined I & II: Turbulence modified by Precipitation". The slide contains two columns of bullet points. The left column discusses Farley-Buneman (FB) turbulence during precipitation, with and without precipitation, and includes a mathematical equation. The right column discusses analyzing the problem kinetically, showing reduced FB growth rates and resonant inelastic e⁻-N₂ cross-sections. A participant list on the right side of the screen shows 11 panelists and 86 attendees.

**Combined I & II:
Turbulence modified by Precipitation**

- What happens to regions with Farley-Buneman (FB) turbulence during precipitation?
 - Without Precipitation, FB waves start when:
 - $\frac{E_{mag}}{B_0} \approx V_D > \approx C_s (1 + \frac{v_e v_L}{\Omega_e \Omega_i})$
 - This leads to anomalous conductivity.
 - With Precipitation
 - Temperatures rise so C_s increases.
 - A full kinetic analysis shows that the effect is larger than this:
- Analyzing Problem Kinetically including
 - Distribution Functions of Precipitating Electrons
 - Energy dependent cross-sections
- Shows:
 - Reduced FB growth rates
 - More than T effects
 - Resonant inelastic e⁻-N₂ cross-section at 2.5 eV suppresses FB instability
- Problem: Observations show both precipitation and turbulence during storms

Contact: meerso@bu.edu

Participants (97): Panelists (11), Attendees (86)

Participant list (partial): AC Agata Chuchra-Konrad, AN Akifumi Nakayama, AK Anton Kashcheyev, BF Banafsheh Ferdousi, BR Ben Reid, BM Boris Maletckii, BW Boyi Wang, BT Brentha Thurairajah, CW Chen Wu, CS Cheng Sheng, CK Chris Krier, CE Christine E Gabrielse, DD David DeBonis

Year	# of abstract
2018	51
2019	36
2020	37
2021	58

2022 AGU Fall Meeting session

Magnetosphere-Ionosphere-Thermosphere Coupling during Storms and Substorms

Toshi Nishimura, Larry Lyons, Astrid Maute, Daniel Billet

Thanks!

We feel like this GC has been extremely successful!